Simulation study of the effects of HIFU irradiation patterns on thermal lesion to biological tissue

HU DONG[a], GANG LIU[a,b] and GAOFENG PENG[a*]
[a.] School of Information Science and Engineering, Changsha Normal University, Changsha, Hunan, China
[b.] School of Physics and Electronics, Central South University, Changsha, Hunan, China

ABSTRACT: The irradiation pattern of high-intensity focused ultrasound (HIFU) has a significant impact on the therapeutic effect of tumor tissue. In this paper, based on the spheroidal beam equation (SBE) nonlinear acoustics equation and the Pennes bio-heat transfer equation, a thermal lesion prediction model of acoustic-thermal coupling is constructed. The effects of different irradiation patterns, such as HIFU irradiation power and pulse number combination, fractionated heating and sustained heating, and changes in the half-opening angle of a concave spherical ultrasonic transducer on thermal lesion in porcine liver tissue were studied. The research results indicated that the difference in thermal lesion area between the “low power × long pulse” and “high power × short pulse” irradiation pattern was relatively small, and their length and width were almost the same. The area of thermal lesion produced by sustained irradiation of porcine liver tissue by HIFU was significantly larger than the area of thermal lesion produced by fractionated heating. The larger the half-opening angle of the transducer, the larger the thermal lesion area generated by irradiating porcine liver tissue. By selecting appropriate irradiation patterns during HIFU treatment, the optimal thermal lesion area can be obtained in biological tissue.
Keywords: High-intensity focused ultrasound; Therapeutic effect; Pulse number; Lesion

1. Introduction

High-intensity focused ultrasound (HIFU) is a promising technology for treating tumors [1-3]. It has the advantages of being non-invasive, less likely to cause cancer cell metastasis, less patient pain, and fast recovery after treatment. It is superior to surgical surgery in many aspects and has great potential clinical application value and application prospects.

In HIFU surgery, clinicians generally choose the commonly used treatment patterns based on their experience, and large-dose treatment pattern will damage the normal tissue in the acoustic channel, such as skin normal tissue scald or nerve injury and other complications, which will bring pain to the patients. However, smaller-dose treatment pattern will cause incomplete lethality of the tumor tissue, which will increase the likelihood of postoperative recurrence [4-6]. Therefore, how to choose the appropriate treatment pattern, which can kill the tumor tissue without damaging the surrounding healthy tissue, is the key to clinical treatment.

In order to effectively increase the treatment area of HIFU, Fan et al. [7] studied the effect of multiple ultrasound treatments on near-field heating in 1996 by changing the delay time between sustained pulses and the motion mode of the transducer in the focal plane. Research has found that in order to avoid normal tissue lesion, it is necessary to have

*Corresponding author.. Tel: +86-0731-84036108; E-mail address: 314644054@qq.com

sufficient delay time between sustained pulses, which is related to sound power and pulse duration. In 2000, Salomir et al. [8] used magnetic resonance imaging (MRI) to guide the HIFU transducer to move along a double helix curve trajectory, and obtained a uniform temperature rise of a certain volume in simulated tissue models, in vitro fresh meat tissue, and in vivo rabbit thighs. In 2009, Kolher et al. [9] utilized a multi element phased transducer to electronically control the ultrasonic beam to generate multiple focal points and move outward along a concentric circle, resulting in a uniformly distributed large-scale thermal lesion to the muscles of the porcine leg. In 2012, Zhou [10] conducted HIFU experiments using simulated tissue models and isolated bovine liver tissue, aiming to shorten treatment time by optimizing the focused ultrasound irradiation path and irradiation time interval. In 2013, Partanen et al. [11] obtained the preset temperature distribution in the target area of tissue mimicking phantom, rabbit thigh muscle and other tissue by using an MRI-guided ultrasound treatment system in combination with multi-focus irradiation and hyperthermia. Vincenot et al. [12] divided the 256-element transducer into eight parts and focused them to form eight focal points to form a ring. By electronically controlling the ultrasound beam, the radius of the ring and the distance from the transducer can be changed. Through this method, a larger volume of lesion area can be obtained in liver tissue. In 2019, Wang et al. [13] compared the efficacy of pulsed HIFU and sustained HIFU ablation under the same ultrasound irradiation dose and found that pulse irradiation resulted in larger liquefied necrotic areas. At the same dose, compared to sustained HIFU, single pulse HIFU treatment can produce liquefaction necrosis and improve ablation efficiency at a higher duty cycle. In 2020, Andreeva et al. [14] investigated the effect of a series of focused ultrasound pulses generated by a multi-element array on the heating of biological tissue, analyzed the effects brought about by different focal point positions, the number of pulse sequences, and the inter-pulse time delay, and found that the parameters of the pulse string and the perfusion process have a significant impact on the size of the area of thermal lesion within the tissue. In 2021, Singh et al. [15] investigated the effects of different duty cycles and ultrasound powers on the thermal response and the corresponding thermal dose distribution during HIFU treatment and found that as the pulse width decreases, the peak temperature and rate of warming decrease accordingly. Pulsed ultrasound was able to increase the volume of necrotic injury within the same ultrasound time. In 2023, Zhu et al. [16] investigated the comparison of the different HIFU pulse repetition frequencies, duty cycles, and frequency differences in the area of in vitro lesion, and the results showed that different pulse parameters lead to different types of lesion. Zhao et al. [17] investigated the relationship between acoustic focal zones and biofocal zones for different combinations of power and time, and found that in low-power cumulative HIFU treatments, when the length of the biofocal zone and the length of the acoustic focal zone were roughly equal, the shape of lesion in the biofocal zone induced by high power with short irradiation was closer to the acoustic focal zone than that in the biofocal zone induced by low power with prolonged irradiation. In 2024, Huang et al. [18] designed a dual-frequency HIFU transducer operating at 4.5 MHz and 13.7 MHz for body-mode and ex vivo tissue testing, and compared the difference in the area of thermal lesion induced by single-frequency ultrasound and dual-frequency ultrasound and found that the use of dual-frequency ultrasound led to a larger area of lesion as compared with frequency ultrasound.

In this paper, the acoustic-thermal coupling model [19] constructed by nonlinear

spheroidal beam equation (SBE) model and Pennes bioheat conduction equation was used to simulate the thermal lesion generated by HIFU irradiation of biological tissue. The effects of three different irradiation patterns, namely, HIFU power and pulse combination, fractionated and sustained heating, and transducer half-opening angle variation, on the thermal lesion of biological tissue were investigated separately, and the relationships between various irradiation patterns and the change in thermal lesion area were investigated. The results of this study are expected to provide theoretical references for the development of safe and effective HIFU preoperative treatment programs.

2. Materials and Methods

2.1 SBE nonlinear sound propagation model

The SBE model is used to calculate the nonlinear sound field distribution of large angle transducers , and it is used to explain the nonlinear ultrasound propagation in the oblate spheroidal coordinate with $-\infty < \sigma < +\infty$, $0 < \eta < 1$, $0 \le \varphi \le 2\pi$. The transformation relationship between ellipsoidal coordinates (σ, η, φ) and rectangular coordinate system (x, y, z) is $x = b\sqrt{[(1+\sigma^2)(1-\eta^2)}\cos\varphi$, $y = b\sqrt{[(1+\sigma^2)(1-\eta^2)}\sin\varphi$, $z = b\sigma\eta$, where the interfocal length is $2b$ [20,21]. The sound field is divided into two parts: the spherical wave approximation region near the surface of the transducer and the plane wave approximation region near the focal point. For the approximate region of spherical waves [21]:

$$\frac{\partial^2 P}{\partial \tau_s \partial \sigma} + \frac{1}{2}\frac{\sin 2\theta}{\sigma(1+\sigma^2)}\frac{\partial^2 P}{\partial \tau_s \partial \theta} + \frac{\varepsilon\sqrt{\sigma^2+\sin^2\theta}}{\sigma(1+\sigma^2)}\left(\frac{\partial^2 P}{\partial \theta^2} + \cot\theta\frac{\partial P}{\partial \theta}\right) + \frac{E}{\sigma}\frac{\partial P}{\partial \tau_s} = -\frac{\sqrt{\sigma^2+\sin^2\theta}}{\sigma}\left(\alpha b\frac{\partial^3 P}{\partial \tau_s^3} + \frac{b}{2l_D}\frac{\partial^2 P^2}{\partial \tau_s^2}\right)E \qquad \sigma < \sigma_0 < 0 \tag{1}$$

The approximate region of plane waves can be expressed as [21]:

$$\frac{\partial^2 P}{\partial \tau_p \partial \sigma} - \frac{\sigma\sin\theta}{1+\sigma^2}\frac{\partial^2 P}{\partial \tau_p \partial \theta} - \frac{\varepsilon(2-\cos\theta)}{1+\sigma^2}\left(\frac{\partial^2 P}{\partial \theta^2} + \cot\theta\frac{\partial P}{\partial \theta}\right) = \left(\alpha b\frac{\partial^3 P}{\partial \tau_p^3} + \frac{b}{2l_D}\frac{\partial^2 P^2}{\partial \tau_p^2}\right)E \qquad \sigma \ge \sigma_0 \tag{2}$$

Due to the axial symmetry of the spherical shell coordinate system, the variable φ is omitted from the equation. The angle variable θ is associated with η as $\eta = \cos\theta$, $\tau_s = \omega[t + b\sqrt{(\sigma^2+\sin 2\theta)}/c_0]$, $\tau_p = \omega[t - b\sigma\cos\theta/c_0]$. $\varepsilon = 1/2kb$, and E is the function of σ and θ as $E(\sigma,\theta) = (\sigma^2+\cos 2\theta)/(1+\sigma^2)$. For a planar wave, $l_D = \rho_0 c_0^3/\beta p_0\omega$ is the shock creation distance, $\alpha = \delta\omega^2/2c_0^3$ is the sound attenuation coefficient, δ is the sound diffusivity, and ω is the angular frequency. Normalized sound pressure is denoted by $P = p/p_0$, and p_0 stands for the sound pressure amplitude on the source surface, c_0 for the sound speed, ρ_0 for the medium density, β for the nonlinear coefficient of the medium, and k for the wave number.

Equations (1) and (2) are solved using a time-frequency domain combination method [22]. By using operator separation, equations (1) and (2) can be simplified as [22]:

$$\frac{\partial^2 \overline{p}}{\partial \tau \partial \sigma} = G(\sigma,\theta)\frac{\partial^2 P}{\partial \tau \partial \theta} + H(\sigma,\theta)(\frac{\partial^2 P}{\partial \theta^2} + \cot\theta \frac{\partial P}{\partial \theta}) + R(\sigma,\theta)\frac{\partial P}{\partial \tau} + S(\sigma,\theta)\frac{\partial^3 P}{\partial \tau^3} \quad (3)$$

$$\frac{\partial P}{\partial \sigma} = N(\sigma,\theta)\frac{\partial P^2}{\partial \tau} \quad (4)$$

The coefficients $G(\sigma,\theta)$, $H(\sigma,\theta)$, $R(\sigma,\theta)$, $S(\sigma,\theta)$, and $N(\sigma,\theta)$ can be derived from equations (1) and (2). Equation (3) is computed in the frequency domain, utilizing the axial distance σ as the boundary condition [22], and equation (4) is resolved using the NT scheme finite-difference method in the time domain [22]. The mean of $P(\sigma,\tau)$ within each step in the time τ direction can be written as [22]:

$$\overline{P}(\sigma,\tau) = \frac{1}{d\tau}\int_{\tau-d\tau/2}^{\tau+d\tau/2} P(\sigma,t)dt \quad (5)$$

If $\overline{P}_j^m$ represents $\overline{P}(m\times d\sigma, j\times d\tau)$, $\overline{P}_j^{m+1}$ can be represented by a NT type difference as [22]:

$$\overline{P}_{j+1/2}^{m+1} = \frac{\overline{P}_j^m + \overline{P}_{j+1}^m}{2} + \frac{d\tau}{8}((P_\tau)_j^m - (P_\tau)_{j+1}^m) - \frac{d\sigma}{d\tau}[f(P_{j+1}^{m+1/2}) - f(P_j^{m+1/2})] \quad (6)$$

Where $f(P) = -N(\sigma,\theta)P^2$ is a nonlinear term. The sound intensity at the focal point is defined as follow [23,24]:

$$I = \sum_{i=1}^{N} |P_i^2| / 2\rho_0 c_0 \quad (7)$$

P_i represents the ith order harmonic pressure amplitude and N is the number of harmonic orders. Sound intensity is positively correlated with temperature increase and thermal lesion [25]. The SBE equation was used in the simulation to calculate the sound field of the HIFU, in which the generation of sound intensity plays a decisive role in the formation of the temperature field, leading to irreversible coagulative necrosis of the diseased tissue [26,27].

2.2 Pennes biothermal conduction model

The thermal effect of HIFU increases the local temperature of the target area, and the Pennes equation is used to calculate the temperature field distribution at the focal region in biological tissue, and for simplicity of calculation, the blood perfusion rate was neglected here. [24, 28].

$$\rho_0 C\frac{\partial T}{\partial t} = k\nabla^2 T + Q \quad (8)$$

Where T is the temperature, C and k represent the heat capacity and thermal conductivity of the tissue. Generally there is a thermal relaxation effect on biological tissue, which can have an effect on the heating of biological tissue. The Pennes equation assumes that biological tissue is homogenous and isotropic [29], which is based on the Fourier heat conduction model, and it does not take into account the thermal relaxation time. However, the non-Fourier heat conduction model considering thermal relaxation time, and the thermal relaxation time in biological tissue is approximately 10^{-8}~10^{-12} seconds for homogeneous medium [30]. It can be seen that when the relaxation time of biological tissue is small, the two models are relatively close. In this paper, the commonly used Pennes equation based on

the Fourier model is used to simplify the calculation. It has been shown that the Pennes equation is suitable for examining temperature distributions, especially those that are at steady state in biological tissue [31-33]. Q is the thermal deposition source related to the sound field, calculated as follows [24]:

$$Q = 2\alpha I \quad (9)$$

Where α is the attenuation coefficient corresponding to the frequency f, and I is the sound intensity.

2.3 Equivalent heat dose

The equivalent heat dose calculation formula is as follows [34]:

$$t_{43} = \sum_{t=0}^{t=final} R^{(43-T_t)} \Delta t \quad (10)$$

In formula (10), T_t is the temperature at time t, R is a constant, R=0.5 (T>43 ℃), R=0.25 (T<43 ℃). This paper defines the lesion area, where the equivalent heat dose is greater than 240 minutes as the coagulation necrosis area of biological tissue.

2.4 Simulation model and parameters

A two-dimensional axisymmetric geometric model of a HIFU transducer irradiating liver tissue was developed, as shown in Figure 1. The inner radius of the HIFU transducer b = 2 cm, the outer radius a = 3.2 cm, the irradiation frequency f = 1 MHz, the geometric focal length F of the transducer, the irradiation power P, pulse number n of the ultrasonic signal, the half-opening angle γ of the transducer, the ultrasound transmission distance z_w in water and the thickness z_l of the liver were all adjustable parameters. r and z represented the radial and axial directions of the HIFU transducer, respectively. The transducer and porcine liver were completely submerged in water. Because of its acoustic impedance similar to that of human tissue, water, as the acoustic wave propagation medium for HIFU therapy, can effectively reduce the reflection loss of acoustic waves at the tissue interface and enhance the penetration of acoustic waves. In addition, the speed of sound characteristic of water was favorable to the focusing of acoustic waves, which enhanced the focusing efficiency of the HIFU transducer. As a biocompatible and non-invasive medium, water also had a cooling function, which helped to protect the transducer and surrounding tissue from overheating damage [35,36].

Figure 1. Geometric model of HIFU irradiated porcine liver

Simulation and calculation of thermal lesion were carried out using MATLAB R2018b software (MathWorks, Natick, Massachusetts, United States). The acoustic and thermal parameters of the media are given in Table 1.

Table 1. Acoustic and thermal parameters of media at 30 ℃ [19,37-39]

3 Simulation results

Thermal lesion is an irreversible coagulative necrosis caused by HIFU irradiation, and the equivalent heat dose approach was developed for numerical simulation. Numerous investigations have proven the method's application in various tissue, as well as its reliability in therapeutic tumor treatment [40,41].

3.1 Effect of power and pulse number on thermal lesion

The initial temperature of the porcine liver and the water was 30 ℃, and the propagation distance of the ultrasonic waves in the water was z_w = 5 cm, and the geometric focal length

was F =6 cm. The ultrasonic pulse duty cycle was 50% and a single pulse duration was 0.2 seconds. Figure 2 shows the comparison of thermal lesion area under different irradiation power and pulse number combinations. The number of HIFU pulses was usually proportional to the irradiation time for a given pulse duration [42,43].

Figure 2. Comparison of porcine liver lesion under different irradiation powers and pulse numbers

Figure 2 shows the lesion map of porcine liver tissue after HIFU irradiation with different power and pulse number combinations. From Figure 2, it can be seen that different combinations of HIFU irradiation power and pulse numbers have certain differences in the size of the lesion area caused by porcine liver tissue. Under the same irradiation power conditions, as the number of ultrasound pulses gradually increased from 100 to 400 (Figure 2 (a) ~ (d)), the thermal lesion area of porcine liver tissue also gradually increased. Under the same pulse number conditions, as the irradiation power gradually increased from 40 W to 70 W (Figure 2 (e) ~ (h)), the thermal lesion area of porcine liver tissue also gradually increased. To further investigate the difference in lesion area caused by different combinations of irradiation power and pulse number on porcine liver tissue, Photoshop software was used to statistically analyze the length and width of the thermal lesion area [44] of porcine liver tissue under the aforementioned conditions of different irradiation power and pulse number combinations. The results are shown in Figure 3.

Figure 3. Comparison of length and width of porcine liver lesion area under different irradiation powers and pulse numbers

From Figure 3, it can be seen that both the pulse number and irradiation power gradually increased, and the length and width of the corresponding thermal lesion area of the irradiated porcine liver tissue also gradually increased. The length and width of the thermal lesion area irradiated by HIFU under the combination of 30 W × 400 pulse were 1.466 cm and 0.485 cm, respectively, while the length and width of the thermal lesion area irradiated by HIFU under the combination of 70 W × 100 pulse were 1.532 cm and 0.455 cm, respectively. It was clear that the length of the lesion produced by the 70 W × 100 pulse irradiation pattern was greater than the length of the lesion produced by the 30 W × 400 pulse, whereas the width of the lesion produced by the 70 W × 100 pulse irradiation pattern was less than the width of the lesion produced by the 30 W × 400 pulse. This is due to the fact that high-power short-duration HIFU irradiation can deposit more energy in a shorter period of time, resulting in a faster rise in tissue temperature and thus longer lesion in the axial direction (the direction of acoustic wave propagation). The width of the lesion in the radial direction (i.e., the transverse direction of the focusing region) may be shorter as a result of irradiation for short periods of time with high power, relative to the axial direction. This may be due to the fact that in the radial direction, the focusing region of the acoustic wave was narrower and the energy distribution was relatively concentrated, whereas the high-power short-duration irradiation strategy reduced the diffusion of the energy in the radial direction, which resulted in a relatively shorter lesion region in the radial direction [42]. It can be seen that for the HIFU irradiation pattern under two different combinations of “low power × long pulse” and “high power × short pulse”, the length and width of the corresponding thermal lesion area of porcine liver tissue were almost the same. The other “high power × short pulse” and “low power × long pulse” combined irradiation modes produced thermal lesion of almost the same length, and similar conclusion was made for the width.

3.2 Impact of fractionated and sustained heating on thermal lesion

To compare the differences in the thermal lesion effects of HIFU fractionated heating and sustained heating irradiation patterns on biological tissue, a thermal lesion simulation study was conducted on porcine liver tissue. HIFU irradiation power P=40 W, ultrasonic

transmission distance in water z_w=5 cm, and geometric focal length of the transducer F=6 cm. For the fractionated heating method, first, the porcine liver tissue was irradiated at 30°C for 2 seconds, and the acoustic and thermal parameters corresponding to the temperature of the porcine liver at 30°C were used to predict the focal temperature, followed by a pause of 0.5 seconds. Subsequently, based on this, the porcine liver tissue was continued to be irradiated using the HIFU for 2 seconds, and the acoustic and thermal parameters corresponding to the temperature of the porcine liver tissue at the end of the previous 2 seconds of irradiation were used to simulate and calculate the area of the thermal lesion. To compare with the fractionated method, porcine liver tissue was sustainedly irradiated by HIFU at 30 ℃ for 4 seconds, and the dynamic acoustic and thermal parameters of the porcine liver were used to predict the thermal lesion area [19]. Through simulation, it can be seen that the temperature after the first heating of fractionated heating is 56.7 ℃, the temperature after the second heating reaches 83.4 ℃. However, the final temperature after one-time heating reaches 89.2 ℃, as shown in Figure 4.

Figure 4. Prediction of focal temperature for fractionated heating and sustained heating

The predicted lesion area for fractionated heating and sustained heating is shown in Figure 5.

Figure 5. Prediction of lesion area by fractionated heating and sustained heating

In Figure 5, the lesion area of porcine liver was predicted by heating the liver from 30 ℃ for 2 seconds and then from 56.7 ℃ for 2 seconds. Compared with the predicted lesion area of porcine liver directly heated from 30 ℃ for 4 seconds, the predicted lesion area of fractionated heating was significantly smaller than the predicted lesion area of sustained heating. The sustained HIFU heating allowed heat to accumulate in the liver tissue due to the lack of cooling intervals, resulting in a continuously expanding area of thermal lesion. Fractionated heating, on the other hand, allowed the liver tissue to dissipate heat between heating cycles, limiting the accumulation and propagation of heat and therefore producing a relatively small area of thermal lesion [45].

3.3 Impact of changes in half-opening angle on thermal lesion

The half-opening angle of HIFU transducers had a significant impact on the focal temperature of biological tissue [46]. There were two ways to change the half-opening angle of spherical focusing transducer, one was to change the transducer aperture while keeping the geometric focal length constant. The other method was to keep the aperture constant while changing the geometrical focal length of the transducer (as shown in the geometrical model of HIFU-irradiated porcine liver in Figure 1). Therefore, the second method was used in this paper to change the half-opening angle of the transducer. For the second method, simulation research was conducted by changing the geometric focal length F of the transducer to 12 cm, 13 cm, and 14 cm, respectively. The transmission distance of ultrasound in water z_w=10 cm, and the corresponding half-opening angles of the focused transducer were γ_1=15.5 °, γ_2=14.3 °, and γ_3=13.2 °, respectively. The irradiation power of the HIFU was P=60W and the irradiation time was 5 seconds. The temperature at the focal point was simulated for the three different half-opening angles mentioned above, and the focal temperatures were 60.6°C, 68.2°C and 76.7°C, respectively, as shown in Figure 6.

Figure 6. Predicted focal temperature under three different half-opening angle

From Figure 6, it can be seen that as the geometric focal length of the transducer increased, i.e., the half-opening angle of the transducer decreased, the maximum temperature obtained by the focal point increased. In the focusing acoustic field of the spherical focusing transducer, the geometric focal length of the transducer increased while the aperture diameter remained

unchanged, the effective radiation area was basically unchanged, i.e., the sound energy was basically unchanged, and at this time, due to the focal point being farther away from the surface of the transducer, the area of the focusing region was smaller, i.e., the acoustic energy per unit area of the focusing area increased, and the temperature rise obtained by the liver layer was increased.

Figure 7. Predicted thermal lesion area under three different half-opening angle

From Figure 7, it can be seen that as the half-opening angle of the ultrasonic transducer increased, the effective radiation area of the transducer, i.e., the sound energy, decreased, resulting in a gradual decrease in its thermal lesion area. That was, when the half-opening angle of the ultrasonic transducer was γ_1=15.5 °, γ_2=14.3 °, and γ_3=13.2 °, respectively, the corresponding thermal lesion area produced was about 0.18 cm^2, 0.39 cm^2 and 0.52 cm^2 , respectively. An increase in the half-opening angle of the transducer (with the transducer aperture held constant) led to an increase in the focusing of the ultrasonic beam and a decrease in the degree of diffusion during propagation, which concentrated the acoustic energy in a smaller area, resulting in a decrease in the size of the thermal lesion area. Due to the diffraction effect of ultrasound, the actual focal point position was closer to the geometric focal point, and the larger the geometric focal length, the more obvious this situation became-that is, the thermal lesion position was closer to the transducer side.

4 Discussion

A theoretical study was conducted on the shape of thermal lesion in porcine liver tissue under different irradiation power and pulse number combinations. Due to the variation of the thermal lesion area with different irradiation power and pulse number combinations, different power and pulse array combinations were used to explore the relationship between the thermal lesion area and the combination of irradiation power and pulse number in low-power cumulative HIFU treatment. In the process of focused ultrasound heating biological tissue, thermal lesion was influenced by factors such as power and pulse number. From the simulation results in Figure 2, it can be seen that the thermal lesion area produced by the “low power × long pulse” irradiation pattern and the “high power × short pulse” irradiation pattern was almost the same, which was similar to the experimental results of Zhao et al. [47], and they found that the thermal lesion area produced by the combination of high acoustic power and short irradiation time was very close to that produced by the combination of low acoustic power and long irradiation time. The reason for this phenomenon was that if thermal lesion area of the same length or width were expected to occur, lower power typically lasted longer pulse irradiation than higher power. Moreover, the lesion area increased with an increasing number of HIFU irradiation pulses (constant power), which was confirmed in the experiment of He et al. [48], and it was found that the higher the acoustic power used for irradiation, the shorter the irradiation time required to achieve a thermal lesion, and there was a positive correlation between the area of the thermal lesion and the irradiation dose (power × exposure time). For smaller tumor tissue, using a “low power × long pulse” irradiation pattern can sometimes achieve good therapeutic effects. Compared with traditional HIFU treatment modes, sustained low-power cumulative HIFU therapy can achieve better efficacy and reduce harm to patients in the treatment of pancreatic tumors and mucinous fibrosarcoma [47,49]. For larger tumor tissue, the use of a “high power × short pulse” irradiation pattern will increase the effect of heat accumulation and lesion on tumor tissue, not only achieving good therapeutic effects but also reducing the time for patients to endure pain.

The porcine liver tissue at 30 ℃ was sustainedly irradiated with HIFU for 4 seconds, and its thermal lesion area was simulated using the dynamic acoustic and thermal parameters corresponding to the porcine liver tissue at different temperature. To compare with this, the irradiation time was divided into three parts. Firstly, the porcine liver tissue was irradiated for 2

seconds, and the corresponding acoustic and thermal parameters at 30 ℃ were used to simulate and calculate the thermal lesion. Then pause for 0.5 seconds, subsequently, after another 2 seconds of radiation treatment on the porcine liver tissue, the thermal lesion area was simulated and calculated using the acoustic and thermal parameters that corresponded to the temperature of the porcine liver tissue at the end of the first 2 seconds. From the simulation results in Fiure 5, it can be seen that the thermal lesion area obtained using the sustained irradiation pattern was larger than the thermal lesion area obtained using the fractionated heating irradiation pattern, and this was similar to the research results of Coon et al. [50], but they only focused on the acoustic and thermal parameters at constant temperature instead of the dynamic acoustic and thermal parameters for sustained heating. In the late stage of clinical surgery, most tumors undergo irreversible coagulation necrosis under the thermal effect of HIFU. For the remaining small portion of tumors, the fractionated heating treatment pattern can be switched to reduce radiation dose and reduce the risk of health tissue damage caused by overtreatment.

Keeping the radius of the ultrasonic transducer unchanged, but the geometric focal length gradually increased, and the corresponding half-opening angle gradually decreased. The increase in the acoustic radiation force of the focused ultrasound transducer at the focal point is significant when the half-opening angle of the transducer is changed from small to large, and the acoustic radiation force of the transducer at the focal point continues to increase with the increase of the half-opening angle, and the region of higher acoustic radiation force decreases, i.e., the focal region decreases. Therefore, the larger the half-opening angle of the transducer, the smaller the thermal lesion area (as shown in Figure 7), which is positively correlated with the results of Sheng et al. [21], who investigated the effect of the half-opening angle of the transducer on the lesion area and found that the axial and radial length of the lesion area decreased with the gradual increase of the half-opening angle. The axial and radial length of the focal region determine the size of the focal region area, i.e., the larger the focal region, the relatively larger the area of thermal lesion caused [16,51]. It can be understood that when the geometric focal length of the spherical focusing ultrasound transducer is increased, it causes a decrease in the acoustic radiation force and an increase in the effective area of action of the acoustic radiation force. When the initial acoustic pressure is the same, the increase in the geometric focal length of the spherical transducer increases the radiated acoustic power so that the focusing effect is enhanced, the focal region is increased, and the resulting thermal lesion area is enlarged. It can be seen that changing the irradiation pattern of the half-opening angle of the ultrasonic transducer, i.e., changing the acoustic radiation force of the transducer, can achieve the desired thermal lesion effect.

5 Conclusion

This paper investigated the thermal lesion effects of different HIFU irradiation patterns such as irradiation power and pulse number combination, fractionated heating and sustained heating, and transducer half-opening angle changes on porcine liver tissue through the numerical simulation method. The research results indicated that the difference in length and width corresponding to the thermal lesion area generated by “low power × long pulse” and “high power × short pulse” was relatively small. The focal temperature and thermal lesion area generated by fractionated heating were significantly smaller than that generated by sustained heating. The spherical half-opening angle of the ultrasonic transducer was directly proportional to the focal temperature and thermal lesion area. The spherical half-opening angle of an ultrasonic transducer was inversely proportional to the temperature of the focal point and the area of thermal lesion. The research results of this paper are expected to provide theoretical references for the safety and reliability of HIFU treatment. Future study will focus on creating experimental circumstances and conducting experimental tests to validate the simulation results.

Acknowledgments

This work was supported by the Key Project of Hunan Provincial Department of Education of China under grant No. 21A0618, the Changsha Natural Science Foundation Project under grant No. kq2202313, and the "Lotus Talents" Project of Changsha Normal University. The authors sincerely thank the anonymous reviewers for their helpful comments and suggestions.

Reference:

[1]Su, S., Wang, Y., Lo, E. M., et al. "High-intensity focused ultrasound ablation increases tumor specific lymphocytes in prostate cancer", Cancer Research, **84**(6), pp.3845(2024). DOI:10.1158/1538-7445.AM2024-3845.

[2]Zulkifli,D., Manan, H.A., Yahya,N., et al. "The applications of high-intensity focused ultrasound (HIFU) ablative therapy in the treatment of primary breast cancer: a systematic review", Diagnostics, **13**(15), pp.2595(2023). DOI:10.3390/diagnostics13152595.

[3]Haddadi,S., Ahmadian, M.T. "Analysis of nonlinear acoustic wave propagation in HIFU treatment using Westervelt equation", Scientia Iranica, **25**(4),pp.2087-2097(2018). DOI:10. 24200/sci.2017.4496.

[4]Lozinski, T., Filipowska, J., Pyka, M., et al. "Magnetic resonance-guided high-intensity ultrasound (MR-HIFU) in the treatment of symptomatic uterine fibroids—Five-year experience", Ginekologia polska, **93**(3), pp.185-194(2022). DOI:10.5603/GP.a2021.0098.

[5]Khandwala, Y. S., Soerensen, S. J. C., Morisetty, S., et al. "The association of tissue change and treatment success during high-intensity focused ultrasound focal therapy for prostate cancer", European urology focus, **9**(4),pp.584-591(2023). DOI: 10.1016/j. euf.2022. 10.010.

[6]Wang, Y., Gong, C., He, M., et al. "Therapeutic dose and long-term efficacy of high-intensity focused ultrasound ablation for different types of uterine fibroids based on signal intensity on T2-weighted MR images", International Journal of Hyperthermia, **40**(1), pp.2194594 (2023). DOI:10.1080/02656736.2023.2194594.

[7]Fan, X.B., and Hynynen, K. "Ultrasound surgery using multiple sonications—treatment time considerations", Ultrasound in medicine & biology, **22**(4),pp.471-482(1996). DOI:10.1016/0301-5629(96)00026-9.

[8]Salomir, R., Palussière, J., Vimeux, F.C, et al. "Local hyperthermia with MR-guided focused ultrasound: Spiral trajectory of the focal point optimized for temperature uniformity in the target region", Journal of Magnetic Resonance Imaging: An Official Journal of the International Society for Magnetic Resonance in Medicine, **12**(4),pp.571-583(2000). DOI:10.1002/1522-2586(200010)12:4<571::AID-JMRI9>3.0.CO;2-2.

[9]Khler, M.O., Mougenot, C., Quesson, B.,et al. "Volumetric HIFU ablation under 3D guidance of rapid MRI thermometry", Medical physics, **36**(8),pp.3521-3535(2009). DOI:10.1118/1.3152112.

[10]Zhou,Y.F."Generating uniform lesions in high intensity focused ultrasound ablation", Journal of the Acoustical Society of America, **131**(4),pp.3211(2012). DOI:10.1121/1.4729596.

[11]Partanen, A., Tillander, M., Yarmolenko, P.S., et al. "Reduction of peak acoustic pressure

and shaping of heated region by use of multifoci sonications in MR-guided high-intensity focused ultrasound mediated mild hyperthermia", Medical physics, **40**(1),pp.013301 (2013). DOI:10.1118/1.4769116.
[12]Vincenot, J., Melodelima, D., Chavrier, F.,et al. "Electronic beam steering used with a toroidal HIFU transducer substantially increases the coagulated volume", Ultrasound in Medicine & Biology, **39**(7),pp.1241-1254 (2013). DOI:10.1016/j.ultrasmedbio.2013.01.019.
[13]Wang, Y., Wang, Q., Luo, Y.,et al. "Comparative study of pulsed versus continuous high-intensity focused ultrasound ablation using in vitro and in vivo models", Journal of Ultrasound in Medicine, **39**(2),pp.259-271(2020). DOI:10.1002/jum.15098.
[14]Andreeva, T. Y. A., Berkovich, A. E., Bykov, N. Y. E., et al. "High-intensity focused ultrasound: heating and destruction of biological tissue",Technical Physics,**65**(9), pp.1455-1466(2020). DOI:10.1134/S1063784220090030.
[15]Singh, G., Paul, A., Shekharet, H., et al. "Pulsed ultrasound assisted thermo-therapy for subsurface tumor ablation: a numerical investigation", Journal of Thermal Science and Engineering Applications, **13**(4),pp.041007(2021). DOI:10.1115/1.4048674.
[16]Zhu, Q., Liu, C., Liu, L., et al. "Effect of pulse parameters on ablation efficiency in dual-frequency HIFU therapy",Ultrasonics,**134**,pp.07064(2023). DOI:10.1016/j. ultras.2023. 107064.
[17]Zhao, P., Wang, Y., Tong, S., et al. "The Effects of Energy on the Relationship between the Acoustic Focal Region and Biological Focal Region during Low-Power Cumulative HIFU Ablation", Applied Sciences, **13**(7),pp.4492 (2023). DOI:10.3390/app13074492.
[18]Huang, W., Jiao, Y., Li, J., et al. "Evaluation of Dual-Frequency Switching HIFU for Optimizing Superficial Ablation", Ultrasound in Medicine & Biology, pp.1-12(2024). DOI:10.1016/j.ultrasmedbio.2024.02.016.
[19]Dong, H., Liu, G., and Tong, X. "Influence of temperature-dependent acoustic and thermal parameters and nonlinear harmonics on the prediction of thermal lesion under HIFU ablation", Mathematical biosciences and engineering, **18**(2),pp.1340-1351(2021). DOI:10.3934/mbe.2021070.
[20]Fan, T., Chen, T., Zhang, W., et al. "Acoustic characterization of high intensity focused ultrasound field generated from a transmitter with large aperture", AIP Conference Proceedings,**1821**(1), pp.180002,AIP (2017). DOI:10.1063/1.4977665.
[21]Sheng, R.Z, and Zhang, J. "Ultrasonic nonlinear fields generated from transmitters with varied aperture angles", Applied Acoustics, **195**,pp. 108867(2022). DOI:10.1016/j. apacoust. 2022.108867.
[22]Chen, T., Qiu, Y. Y., Fan, T. B, et al. "Modeling of shock wave generated from a strong focused ultrasound transducer", Chinese Physics Letters, **30**(7),pp. 074302(2013). DOI: 10.1088/0256-307X/30/7/074302.
[23]Ji, X., Shen, G., Bai, J. et al. "The characterization of an ultrasound spherical phased array for the ablation of deep-seated tissue", Applied acoustics, **73**(5) ,pp.529-534(2012). DOI:10.1016/j.apacoust.2011.12.008.
[24]Mohammadpour, M., and Firoozabadi,B. "High intensity focused ultrasound (HIFU) ablation of porous liver: Numerical analysis of heat transfer and hemodynamics", Applied Thermal Engineering, **170**, pp.115014(2020). DOI:10.1016/j.applthermaleng.2020.115014.
[25]Zou, X., Qian, S., Tan, Q., et al. "Formation of thermal lesions in tissue and its optimal

control during HIFU scanning therapy", Symmetry, **12**(9),pp. 1386(2020). DOI:10.3390/sym12091386.
[26]Lin, C. K. S., Oehm, L., Liebler, M., et al. "Heating of Polymer Films Induced by HIFU: Study of Acoustic and Thermal Effects", IEEE Transactions on Ultrasonics, Ferroelectrics, and Frequency Control, **67**(6),pp. 1201-1209(2019). DOI:10.1109/TUFFC.2019.2940380.
[27]Guntur, S. R., and Choi, M. J. "Influence of temperature-dependent thermal parameters on temperature elevation of tissue exposed to high-intensity focused ultrasound: numerical simulation", Ultrasound in medicine & biology, **41**(3),pp. 806-813 (2015). DOI:10.1016/j.ultrasmedbio.2014.10.008.
[28]Mortazavi, S., and Mokhtari-Dizaji, M. "Numerical study of high-intensity focused ultrasound (HIFU) in fat reduction", Skin Research and Technology, **29**(1),pp.e13280 (2023). DOI:10.1111/srt.13280.
[29]Liu, J., Chen, X., and Xu, L. X. "New thermal wave aspects on burn evaluation of skin subjected to instantaneous heating", IEEE T. Bio-Med. Eng., **46**(4), pp.420-428(1999). DOI:10.1109/10.752939.
[30]Kaminski, W. "Hyperbolic heat conduction equation for materials with a nonhomogeneous inner structure", ASME J. Heat Transfers, **112**,pp.555–560(1990). DOI: 10.1115/1.2910422
[31]Kim, S. J., Hwang, J. Y., Kim, Y. J.,et al. "Numerical simulation method for prediction of HIFU induced lesions in human tissue: FDTD-LBM",Physics of Wave Phenomena,**31**(1), pp.30-35 (2023). DOI:10.3103/S1541308X2301003X.
[32]de los Ríos Cardenas, L., Bermeo Varon, L. A., and de Albuquerque Pereira, W. C. "Parameter estimation in high-intensity focused ultrasound therapy. International Journal for Numerical Methods in Biomedical Engineering", **38**(5), pp.e3591 (2022).DOI:10.1002/cnm.3591.
[33]Lari, S., Han, S. W., Kim, J. U., ,et al. "Design of HIFU Treatment Plans Using Thermodynamic Equilibrium Algorithm", Algorithms, **15**(11), pp.399(2022). DOI:10.3390/a15110399.
[34]Gholami, M., Haghparast, A., and Dehlaghi, V. "Numerical study for optimizing parameters of high intensity focused ultrasound-induced thermal field during liver tumor ablation: HIFU simulator", Iranian journal of medical physics,**14**(1),pp.15-22(2017). DOI:10.22038/ijmp.2017.19268.1176.
[35]Tang, Y., Chen, L. Y., Zhang, A., ,et al. "In vivo non-thermal, selective cancer treatment with high-frequency medium-intensity focused ultrasound", IEEE Access, **9**, pp.122051-122066(2021). DOI:10.1109/ACCESS.2021.3108548.
[36]Coussios, C., Farny, C. H., Ter Haar, G., ,et al. "Role of acoustic cavitation in the delivery and monitoring of cancer treatment by high-intensity focused ultrasound (HIFU)", International journal of hyperthermia, **23**(2), pp.105-120 (2007). DOI:10.1080/02656730701194131.
[37]Roknabadi, A.K., Farhani, S.D., and Roknabadi, M.K. "A computational study of non-Fourier temperature distribution in HIFU ablation of 3D liver tumor", Journal of Thermal Analysis and Calorimetry, **147**(22),pp.12933-12946(2022). DOI:10.1007/s10973- 022-11469-3.
[38]Mohammadpour, M., and Firoozabadi,B. "Numerical study of the effect of vascular bed

on heat transfer during high intensity focused ultrasound (HIFU) ablation of the liver tumor", Journal of thermal biology, **86**, pp.102431(2019). DOI:10.1016/j.jtherbio.2019.102431.
[39]Mortazavi, S., and Mokhtari-Dizaji, M. "Threshold of Linear and Non-Linear Behavior of High Intensity Focused Ultrasound (HIFU) in Skin, Fat, and Muscle Tissue Using Computer Simulation", Iranian Journal of Medical Physics, **19**(3),pp.181-188(2022). DOI: 10.22038/IJMP.2021.59077.1992.
[40]Silva, R. L., Alaeian, M., and Orlande, H. "Design by stochastic simulations of the thermal ablation treatment of tumors with high intensity focused ultrasound", Numerical Heat Transfer, Part B: Fundamentals, **85**(2),pp.105-130 (2024). DOI:10.1080/ 10407790.2023. 2228022.
[41]Chen, K., Kong, D., Yuan, J., et al. "Asymmetric-backed multi-frequency ultrasonic transducer for conformal tumor ablation", IEEE Transactions on Biomedical Engineering, (2024). DOI:10.1109/TBME.2024.3374722.
[42]Fan, P., Jie, Y., Yang, X., et al. "Impact of cavitation on lesion formation induced by high intensity focused ultrasound", Chinese Physics B, **26**(5),pp.054301 (2017). DOI:10. 1088/ 1674-1056/26/5/054301.
[43]Iwasaki, R., Takagi, R., Tomiyasu, K., et al. "Prediction of thermal coagulation from the instantaneous strain distribution induced by high-intensity focused ultrasound", Japanese journal of applied physics, **56**(7S1),pp. 07JF23(2017). DOI:10.7567/JJAP.56.07JF23.
[44]Wang, M., and Zhou, Y. "High-intensity focused ultrasound (HIFU) ablation by frequency chirp excitation: Reduction of the grating lobe in axial focus shifting", Journal of Physics D: Applied Physics, **51**(28),pp. 285402(2018). DOI:10.1088/1361-6463/aacaed.
[45]Zou, X., Dong, H., and Qian, S.Y. "Influence of dynamic tissue properties on temperature elevation and lesions during HIFU scanning therapy: Numerical simulation". Chinese Physics B, **29**(3),pp.034305(2020). DOI:10.1088/1674-1056/ab6c4f.
[46]Rybyanets, A. N., Naumenko, A. A., Shvetsova, N. A., et al. "Theoretical modeling and experimental study of HIFU transducers and acoustic fields", Springer Proc. Phys,**175**, pp.621-637 (2016). DOI:10.1007/978-3-319-26324-3_44.
[47]Zhao, P., Wang, Y., Wu, Y., et al. "Formation process of thermal damage in a target area of high intensity focused ultrasound and effectiveness analysis of B-ultrasound real-time monitoring", Acta Acustica, **6**,pp.41 (2022). DOI:10.1051/aacus/2022036.
[48]He, X., Xiong, X., Zou, et al. "Study on Therapeutic Dosimetry and Biologic Effect of High Intensity Focused Ultrasound". J. Biomed. Eng,**26**, pp.72-74(2009). DOI:CNKI: SUN: SWGC.0.2009-01-019.
[49]Zhong, X., Hu, X., Zhao, P., et al. "The efficacy of low-power cumulative high-intensity focused ultrasound treatment for recurrent desmoid tumor", Cancer Medicine, **11**(10), pp. 2079-2084(2022). DOI:10.1002/cam4.4573.
[50]Coon, Joshua, Nick Todd, and Robert Roemer. "HIFU treatment time reduction through heating approach optimisation", International Journal of Hyperthermia, **28**(8),pp.799-820 (2012). DOI:10.3109/02656736.2012.738846.
[51]Han, Y., Hou, G. Y., Wang, S., et al. "High intensity focused ultrasound (HIFU) focal spot localization using harmonic motion imaging (HMI)", Physics in Medicine & Biology, **60**(15),pp. 5911-5924(2015). DOI:10.1088/0031-9155/60/15/5911.

Biographies

HU DONG received his B.S. degree in electronic science and technology from Hunan University of Arts and Science in 2005, and his M.S. degree and Ph.D. degree in physical electronics from Hunan Normal University in 2008 and 2020, respectively. Since 2011, he has been a associate
Professor at the School of Information and Engineering, Changsha Normal
University, Changsha. His research interest is HIFU signal processing and ablation simulation analysis.

GANG LIU received the B.S. and M.S. degrees from the School of Physics and Communications Electronics, Jiangxi Normal University,Nanchang, China, in 2003 and 2009, respectively. He is currently pursuing the Ph.D. degree with the School of Physics and Electronics, Central South University, Changsha, China. He has been a Lecturer with the School of Information Science and Engineering, Changsha Normal University, Changsha. His research interests massive multiple-input multiple-output, and acoustic signal processing.

GAOFENG PENG received a B.S. degree in Applied Electronic Technology from Hunan N ormal University, China, in 2001 and a M.S. degree in the Circuit and System Specialty from Hunan Normal University, China, in 2009. Since December 2020, he has been a Professor at t he School of Information and Engineering, Changsha Normal University, Changsha. His rese arch interests include networked control systems, and digital signal processing.

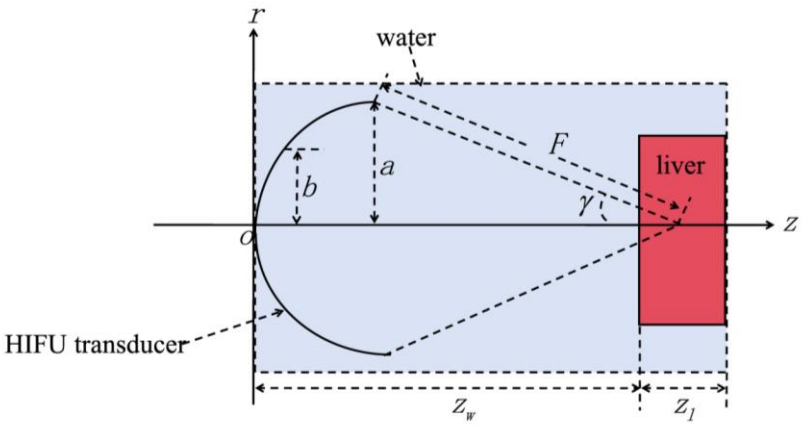

Figure 1. Geometric model of HIFU irradiated porcine liver

Table 1. Acoustic and thermal parameters of media at 30 ℃ [19,37-39]

Material properties	Units	Symbol	Water	Porcine liver
Density	kg/m^3	ρ	1000	1036
Sound velocity	m/s	c	1500	1590
Absorption coefficient	dB/m	α	0.217	70.57
Nonlinear parameter	/	β	3.5	4.3
Specific heat capacity	J/kg/K	C	4180	3604
Thermal conductivity	W/m/K	k	0.60	0.53

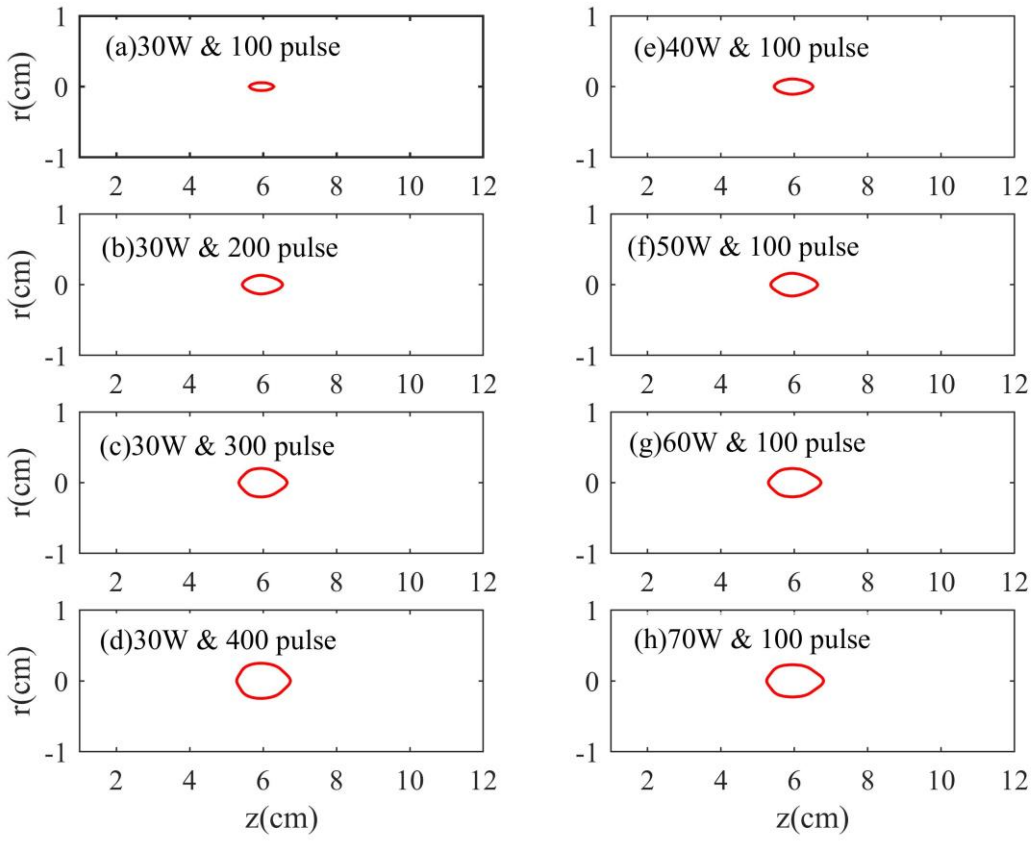

Figure 2. Comparison of porcine liver lesion under different irradiation powers and pulse numbers

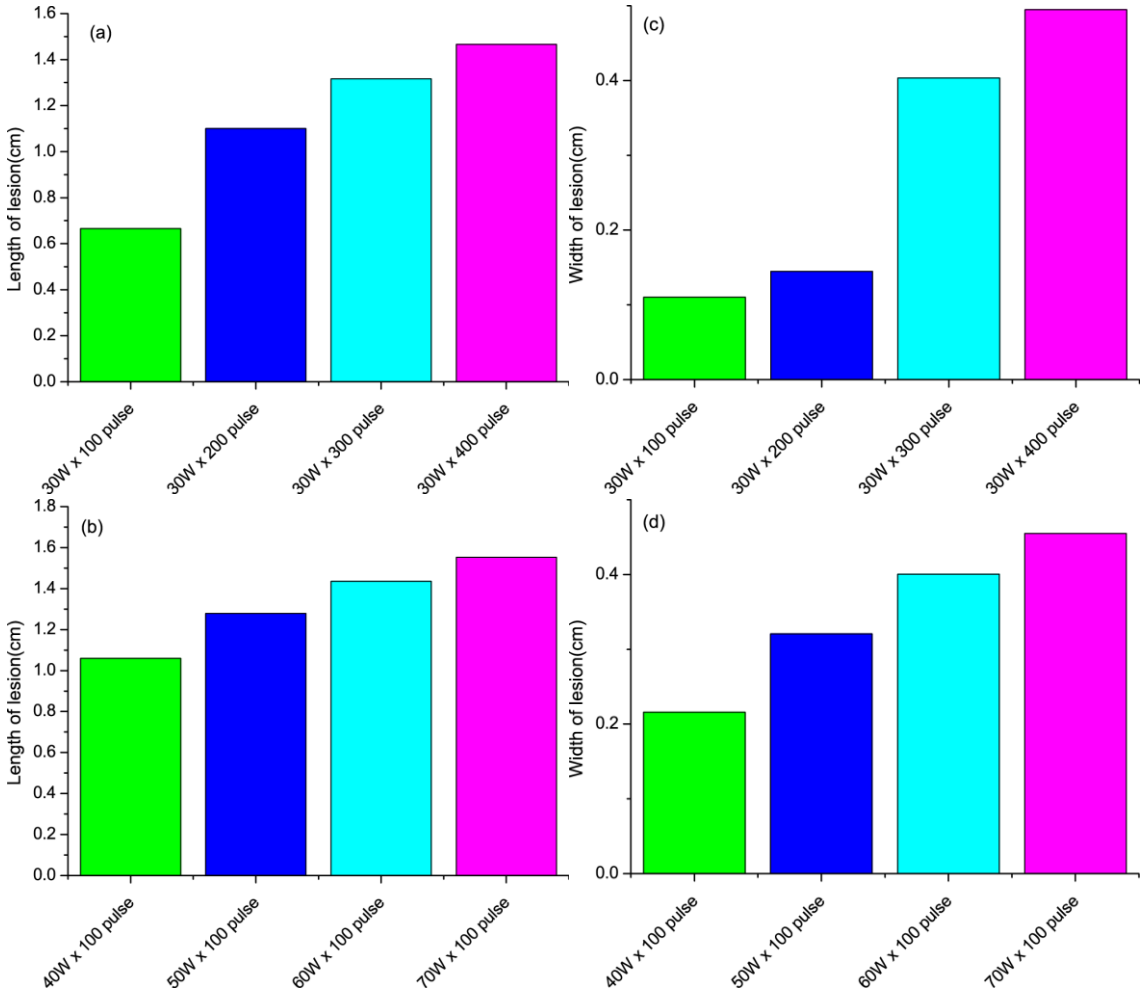

Figure 3. Comparison of length and width of porcine liver lesion area under different irradiation powers and pulse numbers

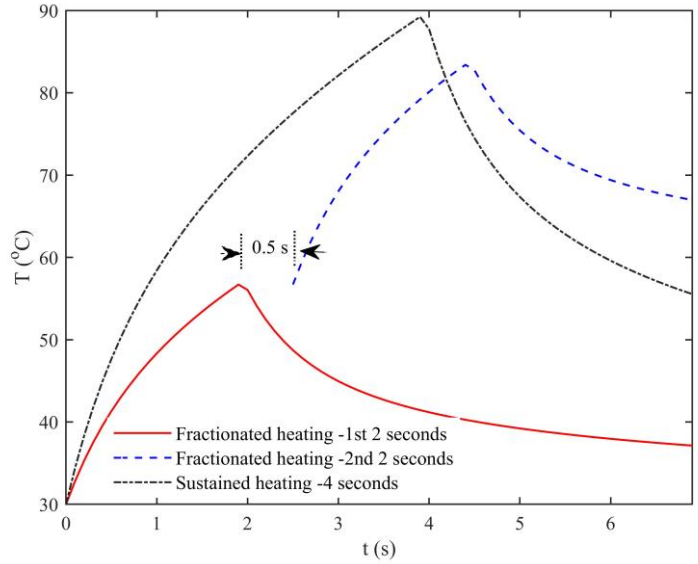

Figure 4. Prediction of focal temperature for fractionated heating and sustained heating

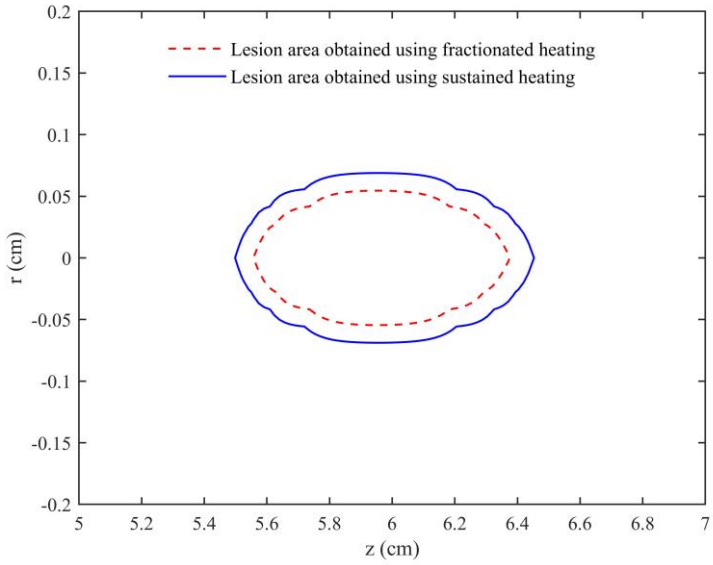

Figure 5. Prediction of lesion area by fractionated heating and sustained heating

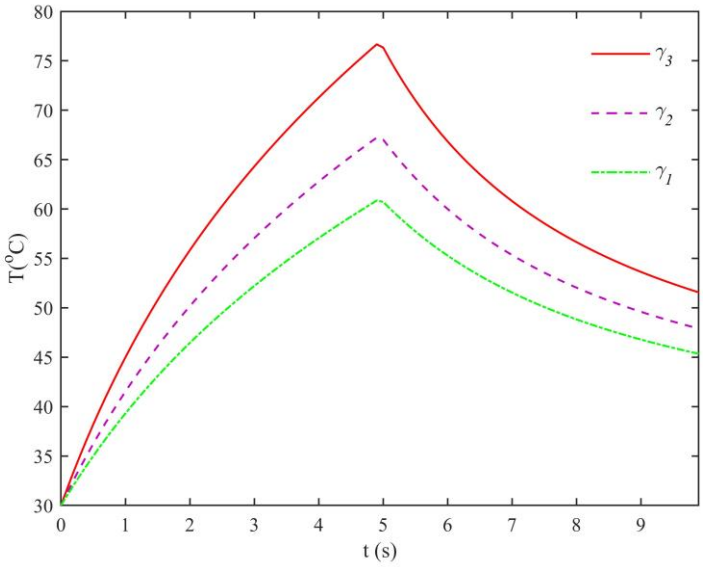

Figure 6. Predicted focal temperature under three different half-opening angle

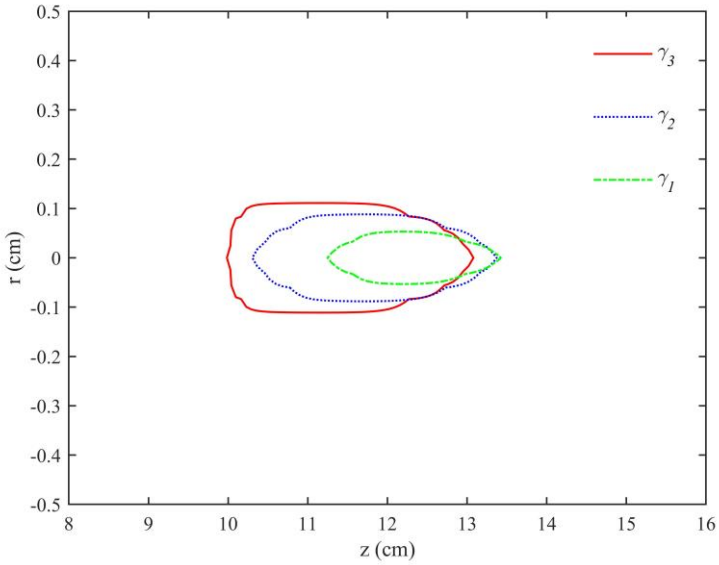

Figure 7. Predicted thermal lesion area under three different half-opening angle